

AN ALL POLYMER AIR-FLOW SENSOR ARRAY USING A PIEZORESISTIVE COMPOSITE ELASTOMER

A.R. Aiyar, C. Song, S.H. Kim and M.G. Allen
Georgia Institute of Technology, Atlanta, GA, USA

ABSTRACT

This paper presents an out-of-plane micromachined piezoresistive flow sensor array based on laser micromachining of polymer films, microstencil printing, and stress-engineered curvature. The developed process is suitable for low cost, large-area sensor array fabrication, and can leverage traditional flex-circuit fabrication. Each device is composed of an out-of-plane curved microtuft formed from laser-machined Kapton® polyimide and PECVD-deposited SiO₂, and a conductive elastomer piezoresistor with a measured gage factor of 7.3 located at the base of the microtuft. The fabrication and performance of a prototype array and a fabrication sequence for large-area arrays on flexible substrates is demonstrated, for flow field mapping across an airfoil. The fabrication sequence also enables backside interconnects without adding further process complexity, which facilitates integration and enables the sensing of airflow with minimum interference due to the sensing circuitry. Individual microtufts as small as 1.5mm in length and 0.4mm in width, with 70 μm wide piezoresistor lines have been fabricated. Wind tunnel testing demonstrated sensitivities as high as 66 Ω/(m/s).

1. INTRODUCTION

Flow sensors are of paramount importance in flight control applications involving unmanned aerial vehicles (UAVs). They essentially consist of out-of-plane structures, such as artificial cilia, or in-plane shear stress sensors [1-3]. Most of these devices are fabricated using silicon, which limits the achievable height of the cilia to well below the boundary layer thickness. This gives little or no information about the flow fluctuations in the main stream [4].

The design of the sensor is based on the extensively studied and reported wind receptor hair in insects [5-6]. Air flow around the hair causes a drag force induced deflection, which in turn activates a sensory response, providing the insect with information about variations in the local flow field. Tall out-of-plane microtufts based on multiple fabrication approaches have been previously demonstrated for this application [5-7].

In this work, we report on the fabrication of a microcantilever based all-polymer flow sensor array with high flow sensitivity, while simultaneously minimizing the need for complex processes. The established fabrication process flow mimics many of the materials and processes in flex-circuit manufacturing, integrating polymer micromachining and laser MEMS techniques. This approach combines the advantages of planar processing with the 3-D capability of a tall out-of-plane flow sensing element in large area arrays on flexible substrates. The elastomer composite piezoresistive material used in the process is also discussed, with an emphasis on its mechanical and electrical characteristics. The fabrication

technique also enables a backside interconnection, which results in minimum intrusion of circuitry into the wind flow.

2. DESIGN AND OPERATION

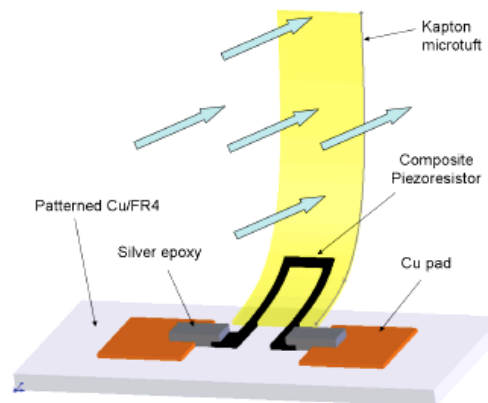


Figure 1: Sensing principle of the microtuft based flow sensor

Figure 1 shows the sensing principle of a prototype sensor. The microtuft itself is fabricated using a thin film of Kapton® (7.6 μm thick, Kapton® 30HN obtained from Dupont). The sensing element is a commercially-available conductive carbon black elastomer with a high piezoresistive gage factor (Elastosil® LR3162, obtained from Wacker Chemie AG), as is demonstrated in this paper. When air flows across the microtuft, it causes deformation of the beam structure and this in turn induces a strain in the piezoresistor. The strain eventually changes the resistance as a function of the applied air flow.

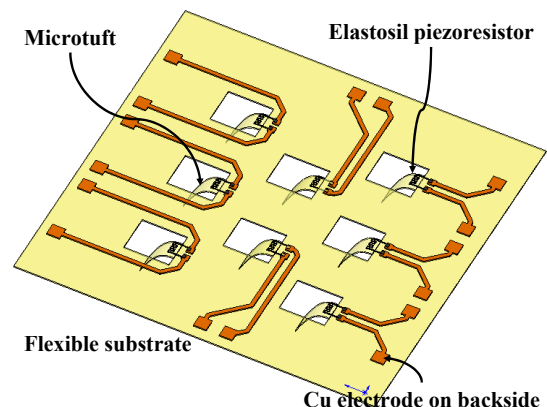


Figure 2: Array of sensors with backside interconnections

Figure 2 illustrates a 3×3 array of the all-polymer flow sensor. The microtuft will have a curvature into the substrate due to the stress-gradient in the material while all the electrical interconnections are placed on the substrate, leading to a backside interconnection scheme.

3. MATERIAL CHARACTERIZATION OF ELASTOSIL® ELASTOMER COMPOSITE

The Elastosil® composite used in the process is a silicone based elastomer loaded with carbon black particles, with a reported volume resistivity of $9 \Omega\text{-cm}$. It is a good candidate for the piezoresistor since it combines a low value of Young's modulus that ensures high values of strain for a given stress and electrical conductivity. In this paper, the Young's modulus and gage factor of the Elastosil® composite material are characterized before implementing the flow sensor array.

Young's Modulus characterization

The Young's modulus of the material is characterized using an Instron (Instron Engineering Corp.) tensile testing instrument.

In order to prepare samples for the tensile testing, a stencil mask is patterned from $12.7 \mu\text{m}$ thick Kapton®, using a CO₂ laser (Gravograph Newhermes), in the form of a rectangular strip of 5 mm width. The LS500XL series CO₂ laser operates at a wavelength of $10.6 \mu\text{m}$ and has a beam spot size of $160 \mu\text{m}$. A low level of energy as well as cutting speed is used to prevent charring. The stencil is then adhered onto a $125 \mu\text{m}$ thick sheet of FEP Kapton® (FEP is Fluorinated ethylene propylene), using a spray adhesive (3M Corp.). The Elastosil® composite material itself, supplied as a two part system, is mixed in a 1:1 ratio of Part A and Part B and cured at a temperature of about $120\text{-}130^\circ\text{C}$ for 2 hours. The two ends of the 5mm wide strip are then placed on two small pieces of FR4 boards and secured in place using a quick cure 2 part epoxy (Loctite Inc.). The FR4 boards are used to prevent any damage to the sample itself by metal clamps in the Instron tool.

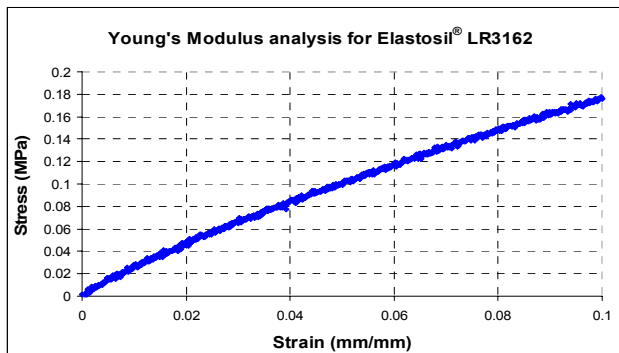


Figure 3: Stress-strain curve for a 5mm wide composite elastomer sample. The thickness of the material is $97 \mu\text{m}$ and the unstrained length is 21mm. The applied strain is 10%.

Once the samples are mounted between the two clamps of the Instron, the tool is programmed to apply a constant strain rate of 0.21 mm/min . A typical stress-strain curve extracted from the load-deflection data obtained from the Instron is shown in Figure 3. The graph indicates that the stress-strain behavior of the composite elastomer is non-linear in nature. The line of best fit has an estimated slope of about 1.9 MPa and it is the approximate Young's modulus of the material.

Characterization of piezoresistive gage factor

The sample making procedure is the same as described in the previous section, except that connection between the material strip and the Cu-FR4 PCB is made using 2 part conductive silver epoxy (Epotek, Ted Pella Inc.). Wires are then soldered onto the PCB to connect the sample to an external resistance measurement unit, which consists of a multimeter (Keithely 196 system DMM), interfaced with a computer that records the resistance real-time, using a data acquisition software (HP-VEE).

The gage factor measurement was performed using a microscope (Nikon MM-40), in conjunction with a multi-axis dimensional measurement instrument (Quadra-Chek 200). The sample is taped onto the side of the microscope such that strains in the elastomer can be applied by rotating the z-axis knob. The corresponding elongation of the sample can be measured using the Quadra-Chek 200. The measurement setup is shown in Figure 4.

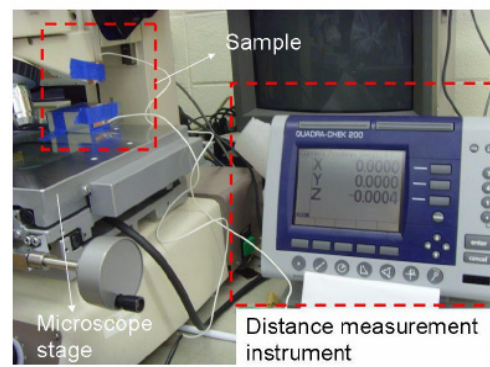


Figure 4: Experimental setup showing sample undergoing tensile testing

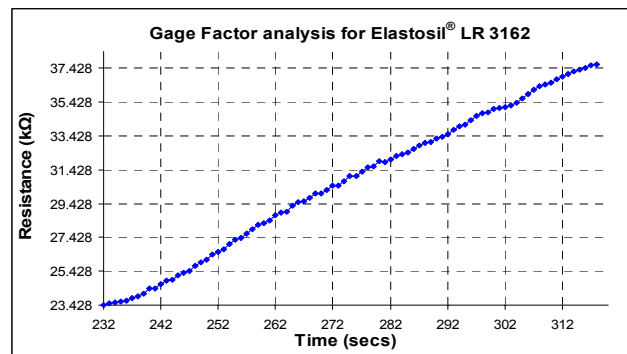


Figure 5: Loading profile for a maximum strain of 10%.

Testing is conducted on a virgin sample strip that has never seen strain. The experiment is started by first ensuring that the sample strip is just taut. Substantial time is allowed for the resistance to stabilize before any strain is applied to the sample. The sample is then continuously strained from 0% to the maximum strain, using the z-focus knob of the microscope. Tests are conducted at 1%, 5% and 10% strains and the corresponding gage factors calculated. A typical tensile test conducted on a $23\text{mm} \times 5\text{mm} \times 0.08\text{mm}$ (LxWxt) is shown in Figure 5.

The gage factor for the elastomer is calculated from the loading profile, as show in Figure 5, using the equation relating the change of resistance to the applied strain [8].

$$\frac{\Delta R}{R} = G\varepsilon$$

The average gage factor (G) calculated from a series of measurements at the above mentioned strains is about 7.3, which is considerably higher than that for metal thin films. It must be mentioned though, that errors could arise in the calculation of the gage factor, since strain values corresponding to each value of resistance are not recorded and the strain rate used is an average value.

4. DEVICE FABRICATION

The process starts with the fabrication of the base or substrate structure. The material for the base is either Kapton® 500HN (for the 1×3 test array) or 300 FN021 (for the larger 3×3 or 5×5 array). The former consists of a $125 \mu\text{m}$ thick Kapton® layer, while the latter consists of a $50.8 \mu\text{m}$ thick Kapton® layer and a $25.4 \mu\text{m}$ thick FEP (Fluorinated ethylene propylene) adhesive layer for lamination purposes.

The first step involves machining of square cavities in the base Kapton®, which act as release holes for releasing the microtufts in the final step (Figure 6(a)). This is achieved by ablating the Kapton® using the CO_2 laser.

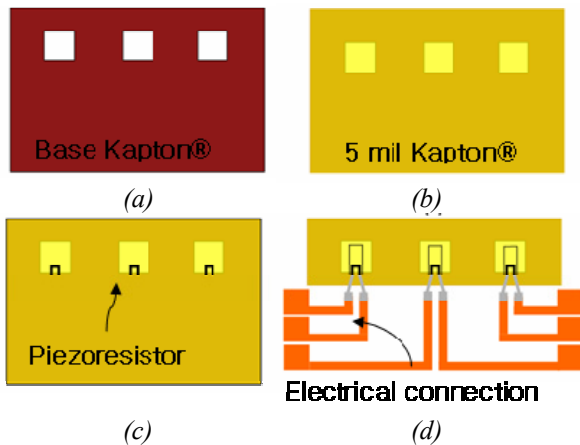


Figure 6: Fabrication process sequence for 1×3 array

The substrate structure or the base is then laminated to the $7.6 \mu\text{m}$ thick device Kapton® layer (Kapton® 30HN) at a temperature of 280°C and a pressure of 1.4 MPa , using a bench top lamination press (Carver Inc.). For the 1×3 array, the substrate layer is adhered to the device layer using a spray adhesive (3M Corp.) (Figure 6(b)).

The next step in the process is patterning the piezoresistive composite material on the laminated substrate. This is achieved by a microstenciling process, whereby the elastomer material is doctor-bladed through a stencil mask onto the substrate. The stencil mask itself is fabricated by the Excimer laser ablation of $12.7 \mu\text{m}$ thick Kapton®. The LPX2000 series excimer laser (Lambda Physik) operates at a wavelength of 248 nm and a spot size of $10 \mu\text{m}$ is obtained through the demagnification optics. After stencil printing of the conductive elastomer, it is cured for about 2 hours at a temperature of 130°C (Figure 6(c)). Interconnections between the conductive elastomers and the external circuit are obtained either using silver epoxy, in the case of the 1×3 array, or

photolithography-based metal deposition for the larger area arrays.

In order to improve the flow-structure interaction, a layer of SiO_2 is deposited on the film using plasma enhanced chemical vapor deposition (PECVD). The residual stress induced due to the oxide deposition produces a curvature in the Kapton®, upon release in the final step of the process (Figure 6(d)).

The final release of the microtufts is achieved using the Excimer laser described before. The laser spot is aligned to features on the substrate and the structure is released by ablating the film. The residual stress causes the microtuft to bend out of or into the plane depending on which side of the substrate the oxide is initially deposited. Figure 7 shows photographs of two devices fabricated with microtuft lengths of 3.5 and 1.5 mm respectively.

The fact that the direction of the curvature (either into or out-of-plane) can be controlled simply by changing the face on which the SiO_2 is deposited, can be used to our advantage for the implementation of the proposed backside interconnects. In this scheme, shown in Figure 8, which is used for the large area arrays, the active circuitry, including all piezoresistors are on the backside of the chip, while microtufts are the only structures that are exposed to the wind flow, causing minimal disturbance of the flow profile.

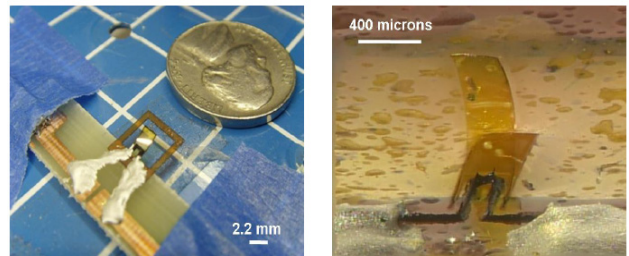


Figure 7: Devices fabricated using the " 1×3 " array fabrication process

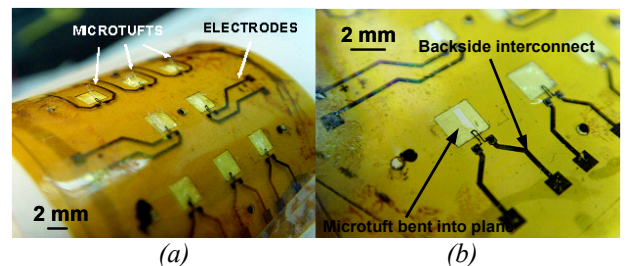


Figure 8: (a) 3×3 flexible sensor array (b) close up demonstrating the backside interconnects. The microtufts are bending into the plane of the paper

5. WIND TUNNEL TESTING

The fabricated devices are tested in a bench top wind tunnel (ST 180 Scantek 2000), shown in Figure 9. The mean free stream velocity in the wind tunnel is measured using a thermal anemometer (Omega FMA-605-I) with a range of $0\text{-}5000 \text{ SFPM}$ ($0\text{-}25 \text{ m/s}$), operating between $4\text{-}20 \text{ mA}$ and this is used as a reference. All the data are recorded in the form of a resistance measurement using a digital multimeter (Keithley).

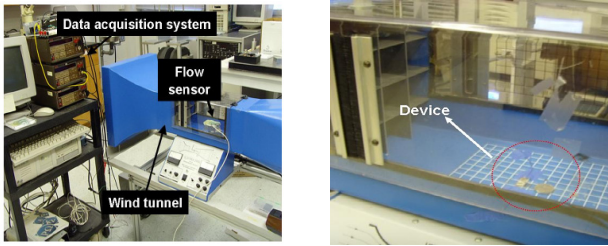


Figure 9: Wind tunnel testing of the fabricated flow sensors

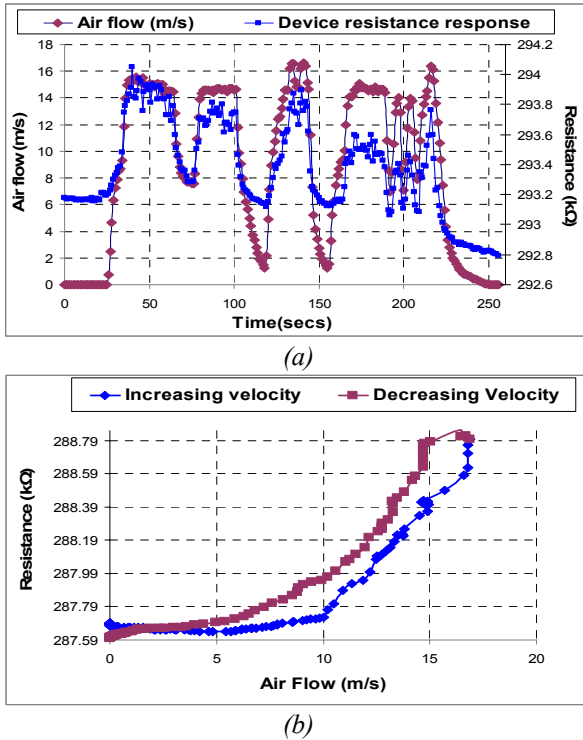


Figure 10: (a) Device response showing correlation between the wind velocity and the resistance profile (b) Device response with increasing and decreasing wind velocity. The device sensitivity calculated from the second graph is approximately $66 \Omega/(m/s)$.

The sensor has a maximum resistance change of about $1.1 \text{ k}\Omega$ leading to a device sensitivity of approximately $66 \Omega/(m/s)$ as shown in Figure 10. The device shows good time response characteristics, though there is resistance hysteresis and drift associated with the piezoresistive response, which may well be the signature of carbon-black elastomer composite materials, as has been extensively reported by other researchers [9,10]. These issues are currently being investigated.

6. CONCLUSION

The proof-of-concept array demonstrates the simple fabrication, low cost, and significant sensor response offered by this approach. Viable deployment, in concert with interface circuitry on the backside, is further supported by its backside interconnect scheme, keeping the circuit elements from interfering with the measured flow, while simultaneously affording the extra protection of the sensor and circuitry. The fabrication has also been extended to large area (3×3) arrays on flexible circuits.

Table 1: Characteristics and performance of the microtuft based flow sensor

Device dimensions	$1.5 \text{ mm (l)} \times 0.4 \text{ mm (w)} \times 7.6 \mu\text{m (t)}$
Maximum change in device response	$\sim 1.1 \text{ k}\Omega$
Maximum change in windflow	16.9 m/s
Sensitivity	$66 \Omega/(m/s)$

ACKNOWLEDGEMENTS

This work was supported in part by the U.S. Air Force under the Multidisciplinary University Research Initiative.

REFERENCES

- [1] A. L. Huang, J. Tai, and C. M. Ho, "Microsensors and actuators for macrofluidic control," *Sensors Journal, IEEE*, vol. 4, pp. 494-502, 2004.
- [2] F. Jiang, G. B. Lee, Y. C. Tai, and C. M. Ho, "A flexible micromachine-based shear-stress sensor array and its application to separation-point detection," *Sensors & Actuators: A. Physical*, vol. 79, pp. 194-203, 2000.
- [3] J. Chen, Z. Fan, J. Zou, J. Engel, and C. Liu, "Two-Dimensional Micromachined Flow Sensor Array for Fluid Mechanics Studies," *Journal of Aerospace Engineering*, vol. 16, pp. 85, 2003.
- [4] Z. Fan, J. Chen, J. Zou, D. Bullen, C. Liu, and F. Delcomyn, "Design and fabrication of artificial lateral line flow sensors," *Journal of Micromechanics and Microengineering*, vol. 12, pp. 655-661, 2002.
- [5] Y. Ozaki, T. Ohyama, T. Yasuda, and I. Shimoyama, "An air flow sensor modeled on wind receptor hairs of insects," *Micro Electro Mechanical Systems, 2000. MEMS 2000. The Thirteenth Annual International Conference on*, pp. 531-536, 2000.
- [6] R. J. F. Wiegierink, A. Jaganatharaja, R. K. Izadi, N. Lammerink, T. S. J. Krijnen, and J. M. Gijs, "Biomimetic Flow-Sensor Arrays Based on the Filiform Hairs on the Cerci of Crickets," *Sensors, 2007 IEEE*, pp. 1073-1076, 2007.
- [7] Y. H. Wang, C. Y. Lee, and C. M. Chiang, "A MEMS-based Air Flow Sensor with a Free-standing Micro-cantilever Structure," *Sensors*, vol. 7, pp. 2389-2401, 2007.
- [8] S. Senturia, *Microsystem Design*, Kluwer Academic Press, 2002.
- [9] X. W. Zhang, Y. Pan, Q. Zheng, and X. S. Yi, "Time dependence of piezoresistance for the conductor-filled polymer composites," *Journal of Polymer Science Part B Polymer Physics*, vol. 38, pp. 2739-2749, 2000.
- [10] K. Yamaguchi, J. J. C. Busfield, and A. G. Thomas, "Electrical and mechanical behavior of filled elastomers. I. The effect of strain," *Journal of Polymer Science, Part B, Polymer Physics*, vol. 41, pp. 2079-2089, 2003.